Update of SO$_2$ emission inventory in the Megacity of Chongqing, China by inverse modeling

Xiaoxiao Feng [a,b], Xiaole Zhang [a,b], Jing Wang [a,b,*]

[a] *Institute of Environmental Engineering (IfU), ETH Zürich, Zürich, 8093, Switzerland*
[b] *Laboratory for Advanced Analytical Technologies, Swiss Federal Laboratories for Materials Science and Technology, Dübendorf, 8600, Switzerland*

HIGHLIGHTS

- The emission inventory of SO$_2$, one of the causal factors of SO$_2$ pollution, was estimated from the ground observations.
- The inverse problem was solved by combing air quality models with Bayesian inference.
- The response of the ambient SO$_2$ to SO$_2$ emissions was quantified as linear.
- The updated emissions were more accurate in predicting the SO$_2$ pollution than the baseline.

ARTICLE INFO

ABSTRACT

Chongqing, a metropolitan with over 32 million residents in southwest China, has suffered from SO$_2$ pollution since 1980s. The emission inventory is an important tool to evaluate the SO$_2$ pollution and to design the effective emission reduction policies. The present work developed a scheme to update the obsolescent SO$_2$ emission inventory in Chongqing obtained from Multi-resolution Emission Inventory for China in 2008 (MEIC2008). The updated emission inventory was estimated by integrating the *a priori* knowledge of the baseline emissions and the current observations based on Bayesian inference, in which the source-receptor sensitivities were calculated by the Decoupled Direct Method in Three Dimensions in the Community Multiscale Air Quality Modeling System (CMAQ DDM-3D). An analytical solution of the Bayesian theorem was derived based on the linear response assumption and applied to estimate the actual SO$_2$ emissions. The updated emission inventory was comparable with the most recent MEIC emission inventory in 2016 and 2017, and was in line with the decline trend of SO$_2$ emissions in Chongqing in the last decade. The adjustment of the emissions improved the accuracy in predicting SO$_2$ concentrations with the developed method.

1. Introduction

Air pollution often plagues metropolitan areas. Sulfur dioxide (SO$_2$) is one of the major atmospheric pollutants, indicating rapid industrialization and urbanization. High levels of SO$_2$ pose a risk to human health. During the early development of large cities, the extremely high level of SO$_2$ and sulfurous smog killed or sickened thousands of people in a short time (Davis, 2002; Helfand et al., 2001). Regarding long term effects, SO$_2$ irritates the respiratory system and aggravates symptoms of respiratory and cardiovascular illnesses, which cause over one million premature deaths each year (Chen and Kan, 2008; Pandey et al., 2005; Venners et al., 2003). SO$_2$ can also harm the environment. Combined with water and air, SO$_2$ transforms into the acid rain, damages the

foliage and causes deforestation. The acid rain also erodes the architecture and acidifies waterways (Clarke and Radojevic, 1987; Gaffney et al., 1987; Larssen et al., 2006).

SO$_2$ is released from both anthropogenic and biogenic emissions. The anthropogenic sources dominate the emissions of SO$_2$, contributing to more than 70% of the global SO$_2$ emissions (Whelpdale and Kaiser, 1997). The primary anthropogenic sources of SO$_2$ are mainly fossil-fuel combustion by power plants and industrial facilities, which account for 50% of the total anthropogenic emissions. The eruption of volcanoes and biogenic dimethyl sulfide are the major natural sources of SO$_2$ (Jain, 2015). China is the third largest emitter of anthropogenic SO$_2$ behind India and Russia, emitting 8% of the global anthropogenic SO$_2$, which was 2156 kilotons SO$_2$ in 2019 (Dahiya et al., 2020).

Chongqing, the sixth-largest Chinese city by economy size, located in the southwest of China, has suffered from the acid rain since 1980s. Chongqing has been assigned as the acid rain control area by the national and local governments (Bingjiang et al., 1998). The coal with the sulfur content of 3.5% used to be the major fuel for the traditional industrial Chongqing (Chang, 2022). By desulphurization of the fuel and using natural gas as the coal substitute, the frequency of acid rain declined significantly, from more than 90% in 1980s to 40% in 2018 (Xuan et al., 2021). However, SO_2 pollution is still one of the major environmental concerns in Chongqing.

Despite of the monitoring of the SO_2 concentrations, the emission inventory is one of the important tools to evaluate the SO_2 pollution and to design the effective emission reduction policies. Bottom-up emission inventories, such as Emissions Database for Global Atmospheric Research (EDGAR) (Olivier et al., 1994), Multi-resolution Emission Inventory for China (MEIC) (Li et al., 2017), Regional Emission inventory in ASia (REAS) (Kurokawa and Ohara, 2020), and the emission inventory developed by Peking University (PKU-FUEL) (Shen et al., 2013), tracked the spatial and temporal variations of SO_2 emissions over the past decades. From the existing emission inventories, the global trend of SO_2 emissions is declining due to the emission restrictions in countries such as USA and China (Streets and Waldhoff, 2000; Popp, 2006).

The generic bottom-up method has been applied to establish the emission inventories (Zhang et al., 2019, 2022). Activities producing SO_2 have been summarized and related parameters have been considered, such as emission factors. However, the emission inventories have systematic bias in evaluating the real-time emissions and predicting air pollution. For instance, EDGAR v4.3.2 was estimated to have annual uncertainties on SO_2 varying between 14.4% and 47.6% in 2012 (Crippa et al., 2018). The uncertainties of SO_2 emissions in MEIC were also significant, up to 30% in Asia in 2012 (Hong et al., 2017). When considering a smaller scale, the spatial bias can be even larger (Zheng et al., 2017). Moreover, all the emission inventories have lags between the available time of the data set and real-time calculation needs. For instance, EDGAR has not been updated since 2012 and the latest public version of MEIC was in 2017, which poses challenges for calculation of the current air pollution due to the temporal uncertainties.

The top-down methods can estimate SO_2 emissions from observations. Researches on updating emission inventories mainly focus on the greenhouse gases, such as carbon dioxide (CO_2) and methane (Thompson et al., 2015; Mazzanti et al., 2006; Feng et al., 2021). The observations from satellite measurements can be used to estimate the SO_2 emissions. The method benefits from the large spatial coverage, but has limitations on data retrieval uncertainties in the conversion of columnar to surface information (Qu et al., 2019; Lee et al., 2011). A previous study updated the SO_2 emissions with the ground observations, but ignored the effects of observations in other regions (Bae et al., 2020). The Decoupled Direct Method in Three Dimensions (CMAQ-DDM-3D) can calculate the sensitivity of ambient pollutants to the predefined emissions, and has been used to estimate the source contributions from regions and sectors (Foley et al., 2014; Cohan et al., 2005). It also provides the possibilities to update the emission inventories (Cheng et al., 2021; Cohan, 2004). However, DDM-3D has not been widely adopted for emission update as it has not been widely reported in the literature.

In the present work, the inverse model was used to update SO_2 emissions in Chongqing. The model integrated both the observations as well as the baseline emission inventory provided by MEIC2008. The baseline simulation was conducted with the chemistry transport model. The SO_2 emissions were updated based on Bayesian inference in which the source-receptor sensitivities were calculated by the CMAQ DDM-3D model. The updated emission inventory was validated first, and then compared with the more recent MEIC inventory, from which the decline of SO_2 emissions can be observed. The updated emission inventory predicted the SO_2 pollution with a higher accuracy.

2. Data and methods

2.1. Measurements of ground-level SO2 concentrations

The observation data in Chongqing were obtained from the China National Environmental Monitoring Center. There were 40 monitoring stations, distributed in 39 counties in Chongqing, shown in Fig. 1a. Most of the stations gathered in the southwestern counties, which were also the political and economic center of Chongqing. Some counties possessed more than one monitoring stations, such as the central YuZhong district, while other mountainous counties had no observation station, such as the northern WuXi county. The observations were averaged monthly as one representative value in the counties with multiple monitoring stations. Since the information of the device performance was difficult to be obtained from Chinese monitoring stations, the observation uncertainties were estimated by calculating the standard deviations among the monitoring stations in the same county.

The monitoring stations recorded the hourly and daily average pollutant concentrations, such as $PM_{2.5}$, PM_{10}, SO_2, NO_2, O_3, CO and also an Air Quality Index (AQI). The SO_2 concentrations were collected in all the monitoring stations within the calculation domains (Fig. 1) in 2021. The measurement methods were UV fluorescence analyzer or differential optical absorption spectroscopy according to China's ambient air quality standards GB 3095–2012. Cubic spline interpolation was applied when the data set had null values. We discarded the data sets that contained only null values.

The measurements were utilized to update the emission inventory by maximizing the *a posteriori* probabilities of the model results being real. However, the uneven distribution of observation stations caused the absence of constraints in some counties when updating the SO_2 emissions.

2.2. Baseline emissions

Emission inventory is the indispensable input data for air quality models. This study employed the Multi-resolution Emission Inventory for China version 1.3 (MEICv1.3) as the baseline emission inventory (Li et al., 2017). MEIC is a static anthropogenic emission inventory of major pollutants with the resolution of $0.25° \times 0.25°$, including the emission information from five different sectors in China, i.e. power sector, industry sector, residential sector, transportation sector, and agriculture sector. The time coverage of the currently available MEIC ranges from 2008 to 2017. In this study, the emission inventory from 2008 was adopted as the baseline emissions. The updated emission inventory of SO_2 was compared with the most recent emission inventories, MEIC2016 and MEIC2017, in Section 4.

2.3. Chemistry transport model

Chemistry transport model calculated the pollutant concentrations with the developed emission inventory (Zhang et al., 2020, 2021, 2022; Gao et al., 2022). In the study, we applied the chemistry transport model to calculate the SO_2 concentrations based on the baseline emission inventory and then analyzed the deviations between the simulated SO_2 concentrations and the observations. The chemistry transport model was also used to validate the updated emission inventory.

The combined Weather Research and Forecasting Model (WRF) version 3.8 and Community Multiscale Air Quality Modeling System (CMAQ) version 5.2 were used in the study (United States Environmental Protection Agency, 2020; Skamarock et al., 2008). Driven by the meteorological field generated by the WRF model, the CMAQ system calculated the process of the pollutants' formation, transport, evolution, and removal. In the study, WRF-CMAQ model calculated the pollutant concentrations with the *a priori* knowledge of the baseline and the updated emission inventories.

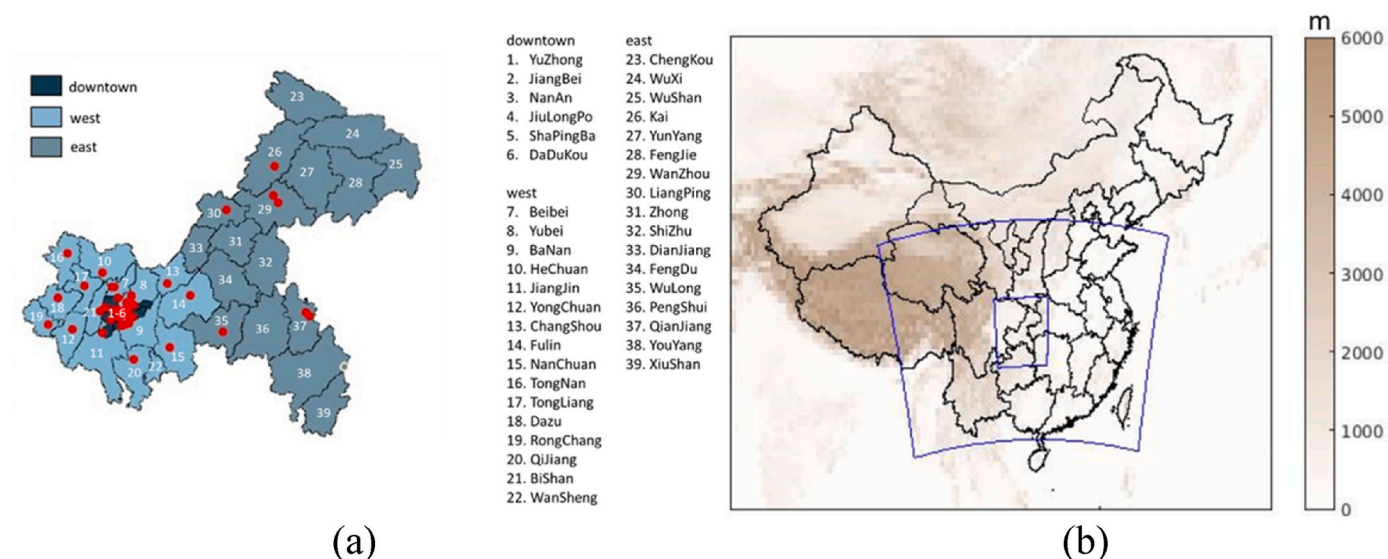In the WRF-CMAQ model, two nested domains were set up using one-

Fig. 1. (a) Observation stations in Chongqing counties. The red dots referred to the locations of the stations. (b) Model domains. The color referred to terrain heights of the two nested model domains with horizontal resolutions of 30 km × 30 km (large domain), and 5 km × 5 km (small domain). (For interpretation of the references to colour in this figure legend, the reader is referred to the Web version of this article).

way nesting in the Lambert Conic Conformal projection with horizontal resolutions of 30 km × 30 km and 5 km × 5 km, respectively, shown in Fig. 1b. The larger domain covered South China. The smaller domain covered Chongqing and some areas of the neighboring provinces. The choice of the horizontal grid setting was a compromise between the accuracy of problem solving and the limitation of the computational power. The grid of the large domain was coarse to reduce the calculation time. Two domains were set instead of three. The intermediate domain was omitted due to the limitation of the computational power. The resolution of the small domain should be fine enough for the question. However, the fine grid would increase the calculation time dramatically, especially in calculating the sensitivity matrix (See Section 2.4.2). Currently, it would not be feasible to use a finer grid than 5 km for the small domain. The simulation utilized 30 terrain-following σ-levels up to 10 hPa (i.e., ~20 km a.s.l.). The land use information was obtained from the MODIS (Moderate Resolution Imaging Spectroradiometer) IGBP (International Geosphere–Biosphere Programme) 21-category data (ORNL DAAC, 2018). Sparse Matrix Operator Kernel Emissions Modeling System (SMOKE) version 4.5 was used to preprocess the baseline MEIC emission inventory before running the chemistry transport model CMAQ (Coats, 1996). The emission inventory was re-gridded to match the spatial and temporal configurations of CMAQ. The pollutants from the emission inventory were classified into more specific species to fit the CMAQ chemical mechanism.

Table 1
Configuration of WRF and CMAQ.

WRF	
Initial field	NCEP FNL
Microphysics	WRF Single-Moment (WSM) 3-class simple ice
Cumulus scheme	Kain-Fritsch
Land surface model scheme	Noah
Planetary boundary layer scheme	Yonsei University (YSU) planetary boundary layer (PBL)
CMAQ	
Chemical mechanism	cb05e51
Chemical solver	Euler Backward Iterative (EBI)
Aerosol module	aerosol6
Advection scheme	Yamartino (YAMO)
Horizontal diffusion	multiscale
Vertical diffusion	Asymmetric Convective Model version 2 (acm2)
Cloud scheme	acm_ae6
Initiation	Default profile

The configuration information of WRF and CMAQ was listed in Table 1. WRF was initialized by the meteorological field from the final global tropospheric analyses by National Centers for Environmental Prediction (NCEP) Final (FNL) Operational Global Analysis data. The NCEP FNL data also provided the boundary conditions for the WRF model. For the CMAQ model, the boundary and initial conditions were given by the default profiles embedded in CMAQ. January, April, July and October 2021 were chosen as the simulation periods and represented four seasons. To reduce the influences of the initial conditions, the first 10 days were regarded as the 'spin-up' period of the simulation (Itahashi et al., 2012). Simulation results on the rest days were compared and analyzed. The chemical mechanisms used in the model were Carbon Bond 2005 e51 (CB05e51) and aerosol6. The only chemical reaction related to SO_2 in the mechanisms was

$$SO_2 + OH = SULF + HO_2 + SULRXN \tag{1}$$

where OH was hydroxyl radical, SULF was gaseous sulfuric acid, HO_2 was hydroperoxy radical, and SULRXN was the precursor of aerosol sulfate.

CMAQ-DDM-3D was also used in the study. DDM-3D is a separate version of the CMAQ model that provides an efficient approach for probing the sensitivity of atmospheric pollutant concentrations to various changes in model inputs including emissions (Hakami et al., 2003). The detailed information of DDM-3D was introduced in Section 2.4.2.

2.4. Inverse model

In the logical direction contrary to the CMAQ simulation, it was possible to estimate the emissions with the observations, known as the top-down method. We adopted the inverse model to update the emission inventory based on observations, source-receptor sensitivity and the *a priori* knowledge of baseline emissions. The flowchart of the top-down method was shown in Fig. 2.

2.4.1. Bayesian inference

Bayesian inference was used in the study to yield the maximum probability of the real emission inventory (Bayes, 1763), which has been successfully utilized to estimate the emissions based on observations (Zhang et al., 2014, 2015; Wang et al., 2018). Two datasets were considered, which were the observations $\mathbf{d}^{obs}$ and unknown emission
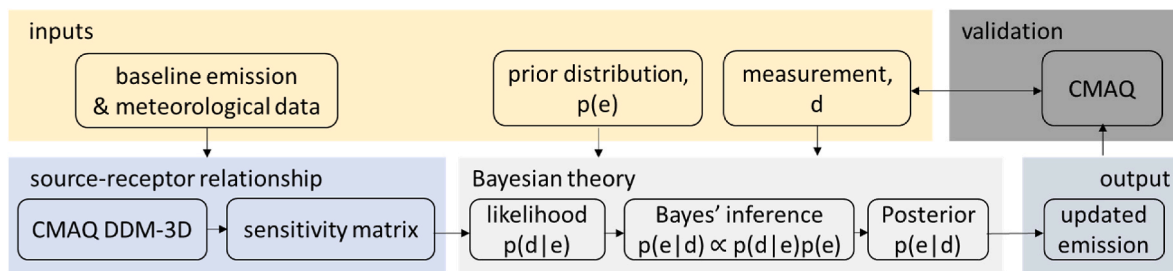
Fig. 2. Flowchart of the emission update method.

parameter **e**. Except for $\mathbf{d}^{obs}$, all the SO_2 concentrations mentioned in Section 2.4 were modeled concentrations. The possibility density of *a posteriori* emissions was given by Bayes' theorem:

$$p\left(\mathbf{e}|\mathbf{d}^{obs}\right) = \frac{p\left(\mathbf{d}^{obs}|\mathbf{e}\right)p(\mathbf{e})}{p\left(\mathbf{d}^{obs}\right)} \tag{2}$$

where $p(\mathbf{d}^{obs}|\mathbf{e})$ was the *a priori* of observed data, also named as the likelihood function, $p(\mathbf{e})$ was the *a priori* of the emissions, $p(\mathbf{d}^{obs})$ was a normalization factor, named as evidence. The evidence scaled the *a posteriori*, and its numerical value did not affect relative likelihoods of the emissions **e**. The *a posteriori* was the solution of the inverse problem. The *a priori* information of the observation data, the baseline emissions, and the source-receptor sensitivity were integrated to estimate the *a posteriori* emissions.

The likelihood function was assumed to be in the form of Gaussian distribution, since the measurement errors were considered to follow the normal distribution. The *a priori* knowledge of the emissions was also described as Gaussian distribution, considering the uncertainties of the baseline emissions.

$$p\left(\mathbf{d}^{obs}|\mathbf{e}\right) = const.e^{-\frac{1}{2}\left(\mathbf{d}-\mathbf{d}^{obs}\right)^T \mathbf{C}_d^{-1}\left(\mathbf{d}-\mathbf{d}^{obs}\right)} \tag{3}$$

$$p(\mathbf{e}) = const.e^{-\frac{1}{2}\left(\mathbf{e}-\mathbf{e}^{prior}\right)^T \mathbf{C}_e^{-1}\left(\mathbf{e}-\mathbf{e}^{prior}\right)} \tag{4}$$

where **d** was the concentrations calculated by CMAQ with the dimension of n (number of the observations) by 1. $\mathbf{e}^{prior}$ was the baseline emissions. $\mathbf{C}_d$ was the covariance matrix of the SO_2 concentrations, and $\mathbf{C}_e$ was the covariance matrix of the emissions. The dimension of the covariance matrixes $\mathbf{C}_d$ was n (number of observations) by n, while the dimension of the covariance matrixes $\mathbf{C}_e$ was m (number of the emission areas) by m. $\mathbf{C}_e$ captured the *a priori* uncertainties of the baseline emissions. $\mathbf{C}_d$ described the observational uncertainties. The detailed construction method of covariance matrices was described in Section 2.4.3. Combined with the probability distribution of the *a priori*, the *a posterior* can be rewritten as:

$$p\left(\mathbf{e}|\mathbf{d}^{obs}\right) = const.e^{\chi(\mathbf{e})} \tag{5}$$

$$\chi(\mathbf{e}) = -\frac{1}{2}\left[\left(\mathbf{d}-\mathbf{d}^{obs}\right)^T \mathbf{C}_d^{-1}\left(\mathbf{d}-\mathbf{d}^{obs}\right) + \left(\mathbf{e}-\mathbf{e}^{prior}\right)^T \mathbf{C}_e^{-1}\left(\mathbf{e}-\mathbf{e}^{prior}\right)\right] \tag{6}$$

We assumed that the response of the ambient concentrations **d** to the emissions **e** was linear. **G** was the source-receptor sensitivity matrix.

$$\mathbf{d} = \mathbf{Ge} \tag{7}$$

When the *a posteriori* had the maximum probability, the estimated emissions can be solved in the following equation:

$$\widetilde{\mathbf{e}} = \left(\mathbf{G}^T\mathbf{C}_d\mathbf{G} + \mathbf{C}_e^{-1}\right)^{-1}\left(\mathbf{G}^T\mathbf{C}_d\mathbf{d}^{obs} + \mathbf{C}_e^{-1}\mathbf{e}^{prior}\right) \tag{8}$$

where $\widetilde{\mathbf{e}}$ was the estimated emissions. the sensitivity matrix described the small change of the SO_2 concentration in response to the small change of the emissions. The generation of the sensitivity matrix was introduced in Section 2.4.2.

2.4.2. Sensitivity matrix

The sensitivity matrix was a Jacobian matrix, describing the response of the SO_2 concentrations to the changes of the emissions. The entry of the sensitivity matrix $G_{(i,j)}$ was the first order derivative of SO_2 concentration **d** at the location *i* with respect to the emission **e** at location *j*, shown in the following equation.

$$G(i,j) = \frac{\partial d(i)}{\partial e(j)} \tag{9}$$

CMAQ-DDM-3D was used to generate the sensitivity matrix in the study. The entries of the sensitivity matrix generated by DDM-3D were the gradient normalized by the local emissions strength **P** (Hakami et al., 2003).

$$G_D(i,j) = P(j)\frac{\partial d(i)}{\partial p(j)} = \frac{\partial d(i)}{\partial[p(j)/P(j)]} \tag{10}$$

where $\mathbf{G}_D$ was the sensitivity matrix generated by DDM-3D. **p** was the emission variable and **P** was the nominal value of **p** used in the simulation.

In our case, the setup of CMAQ-DDM-3D was the same as that of CMAQ in the small domain. When constructing the sensitivity matrix, the small domain was further divided into 41 areas, including 39 counties of Chongqing, the area in the small domain but out of Chongqing (as shown in Fig. 1), and the boundary of the small domain. The sensitivity of SO_2 concentrations responding to the SO_2 emissions in each area was calculated. Therefore, the dimension of the sensitivity matrix was n (number of observations) by m (number of the emission areas, which was 41). The simulation with CMAQ-DDM-3D was conducted after 10 days' 'spin-up' to generate sensitivity matrix. The sensitivity matrix in each month was constructed based on the monthly average.

2.4.3. Covariance design

The design of the covariance matrix was elucidated in the section. The *a priori* covariance matrix described uncertainties of baseline emissions and correlations of emission strength between areas. Data covariance matrix described the measurement uncertainties. The errors of baseline emissions and observations were dispensable for updating the emissions. The errors indicated that the baseline emissions and observations deviated from the reality.

The *a priori* covariance matrix was symmetric. The diagonal elements of $\mathbf{C}_e$ were the uncertainties of baseline emissions in each area, proportional to the *a priori* emissions by a relative uncertainty factor of f_e. f_e was around 15%, estimated by predicting surface concentrations of SO_2 based on MEIC in previous research (Hong et al., 2017; Zheng et al., 2017). Meanwhile, the off-diagonal elements of $\mathbf{C}_e$ were allowed to be non-zero. They showed the correlations of emission strength between two areas. Realistically, it was difficult to acquire the information how the emission strength in one area was correlated with strength in another area. Therefore, an empirical spatial correlation was proposed, depicting the exponential decay with the distance between two areas (Tarantola and Valette, 1982).

$$(C_e)_{ij} = e^{-\frac{|x_i - x_j|}{\lambda}} \sqrt{C_{e,(i,i)}} \sqrt{C_{e,(j,j)}} \qquad (11)$$

where $|x_i-x_j|$ was the distance between the centers of area i and area j. λ was the correlation length. The relative magnitude of $|x_i-x_j|$ and λ determined the gradient of emission strength among areas. When λ was small compared with $|x_i-x_j|$, the emission strength changed rapidly from an area to the surroundings. In contrast, λ with a large value compared with $|x_i-x_j|$ implied that the emission strength in an area correlated with other areas over relatively large distance, and the emission strength changed smoothly. In previous studies, λ was estimated to be around 8–50 km based on comparisons of the spatial structures of multiple emission inventories (Hiller et al., 2014; Henne et al., 2016). The uncertainty of the total emissions was given by $\sigma(E_{tot})$.

$$\sigma(E_{tot}) = \sqrt{\sum_i \sum_j C_{e,(i,j)}} \qquad (12)$$

Both the observation and model uncertainties were contained in the data covariance matrix. The data covariance matrix was also symmetric. The diagonal elements of the matrix were constructed as quadratic form of the observation uncertainties σ_{obs} and model uncertainties σ_{model} in each area, shown as Equation (13). Since the device performance information was difficult to be obtained from Chinese monitoring stations, the observation uncertainties were estimated by calculating the standard deviations among the monitoring stations in the same counties. The model uncertainties were estimated from model residuals. It was assumed that the model uncertainties were various among different locations. However, for each location, the model uncertainties remained constant and were estimated by calculating the root mean square error (RMSE) of the difference between the simulation results and the observations (Henne et al., 2016). The off-diagonal elements of the data covariance matrix were set to 0.

$$C_d(i, i) = \sigma_{obs}^2 + \sigma_{model}^2 \qquad (13)$$

2.4.4. Validation

We validated the updated emission inventory by calculating the value of root-mean-square misfit, shown in the following equation:

$$\chi^{rms} = \sqrt{\frac{1}{N} \sum_{i=1}^{N} (\mathbf{d}^{obs} - \mathbf{d}^{est})^T \mathbf{C}_d^{-1} (\mathbf{d}^{obs} - \mathbf{d}^{est})} \qquad (14)$$

where $\mathbf{d}^{est}$ was the simulated SO_2 concentration with the updated emissions calculated by the linear Equation (7). The root-mean-square misfit compared the SO_2 concentration from simulation and observations. When the simulated results were close to observations and roughly within the observational errors ε, $\mathbf{d}^{obs} - \mathbf{d}^{est} \approx \varepsilon$, and the root mean-square misfit should equal to 1. When χ^{rms} was significantly larger than 1, the difference between the simulations and observations was larger than the observational error. The situation was referred to as under-fitting the data. On the contrary, when χ^{rms} was significantly smaller than 1, the observational error was fitted instead of the credible data, called over-fitting.

Besides, the SO_2 concentrations was calculated based on the updated emission inventory with CMAQ model, and then compared with the observations in order to validate the updated emission inventory directly.

3. Results

3.1. Updated SO_2 emission inventory

3.1.1. Sensitivity matrix

The DDM-3D model probed how the sensitivity of SO_2 concentrations to perturbations in SO_2 emissions propagated through every physical and chemical model in CMAQ. Therefore, the sensitivity matrix presented not only the change of the ambient concentrations in response to the change of emissions, but also included the meteorological information.

Fig. 3 shows the averaged values of the sensitivity matrix in January, April, July and October based on MEIC2008 with the meteorological conditions of 2021. The local emissions contributed more than the remote emissions, since the values of diagonal entries were higher than the off-diagonal ones. The sensitivity matrix can be divided into 3 areas, Chongqing downtown, east Chongqing and west Chongqing. Chongqing downtown had the strongest emissions, followed by the west and east Chongqing. Regarding the gradient of concentrations, the change of the SO_2 concentration to the normalized emission was the highest in downtown, the central area of Chongqing, but lowest in the east, the rural and mountainous Chongqing.

The sensitivity matrix was not diagonally symmetrical, which meant the impact from emissions in area A to the SO_2 concentration in area B was not equivalent to that from B to A. The orientation of emission contribution implied the meteorological and terrestrial conditions. For instance, in July, the emissions from BaNan on the south side of the downtown had a strong impact on the areas in the downtown, such as DaDuKou, JiuLongPo and NanAn. However, the impact of BaNan decreased in January. In the meantime, the emissions from YuBei, located on the north side of the downtown, had increased impact on the downtown. It can be explained by that the prevailing wind in summer was often from south and reversed in winter in Chongqing.

3.1.2. Updated emissions

We updated the SO_2 emissions in Chongqing by integrating the information of observations and the baseline emissions. The gridded emissions from MEIC2008 in each month was aggregated and averaged by county as the baseline. The observations from monitoring stations were also averaged in each county as one representative value.

Fig. 4a shows the baseline emission inventory. The spatial distribution of the baseline emissions was similar to each other in four months, while the emission strength in the same area varied slightly across the year. The downtown Chongqing accounted for the largest amount of SO_2 emissions, followed by the west Chongqing outside of the downtown. The emission strength in the east was the lowest. The emissions in April were higher than the rest of the months, while July was the lowest. However, the observations were not consistent with the temporal variations and spatial profiles of the emissions, shown in Fig. 4b. The observed SO_2 concentrations in the downtown were not significantly higher than the observations in the east. Moreover, the SO_2 pollution was highest in January and lowest in July, not only affected by the emissions, but by the meteorological conditions as well.

Combining the baseline emissions and the observations, we obtained the updated emissions. Adjustment ratios of the updated emissions to the baseline emissions were shown in Fig. 4c. The emissions decreased in all counties after adjustment in the four months, except that the updated emissions in the east counties increased 1%~4% in April. The emissions in the downtown decreased most and the updated emissions were about 10% of the baseline. The emissions from west Chongqing were reduced to 60% compared with the baseline. The emissions from the east remained almost the same after the update. Regarding the temporal variations, the updated emissions were highest in January and lowest in July. The updated emissions became more consistent with the spatial and temporal variations of the observations.

3.2. Validation

To show the improvement of the updated emissions, we compared the deviations of the simulated concentrations based on the baseline and the updated emissions from the observations. The observations and the simulated results were averaged annually in this section. The monthly average of the observations and the simulated results were shown in the
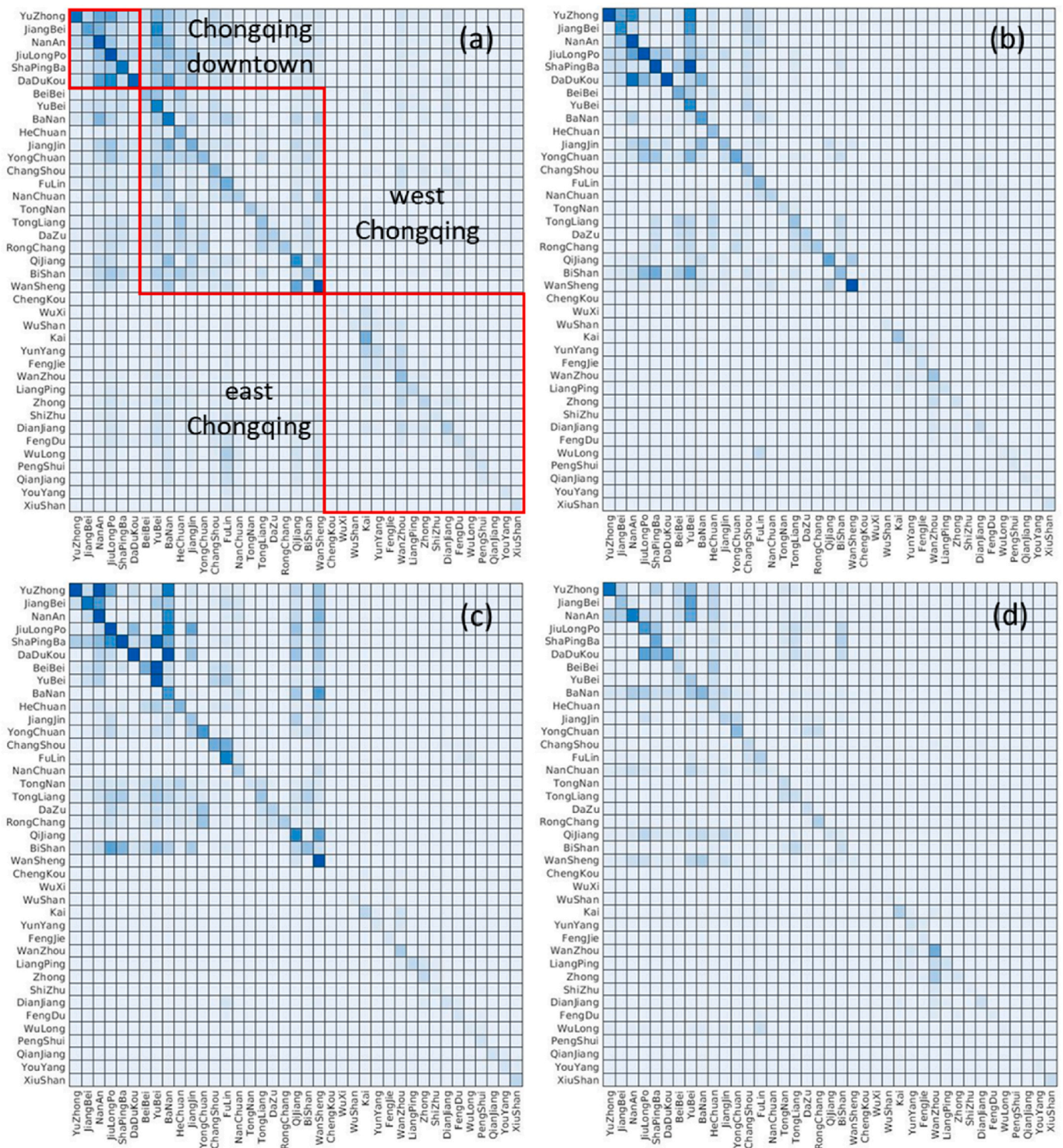
Fig. 3. Sensitivity matrix in 4 months. (a)–(d) were the sensitivity matrixes in January, April, July and October, respectively. The matrix showed the emission impact from 39 counties (x axis) on SO_2 concentrations in the corresponding counties (y axis).

supplementary material.

The observations did not vary abruptly among counties. However, the simulation results based on the baseline showed an abrupt change from the downtown to the east. The area with the highest emission strength was polluted most heavily, while the east had the lightest pollution and the lowest emission strength, shown in Fig. 5(a1). The simulation results based on the baseline were higher than the observations in most counties, and the difference between the observations and the simulation results was largest in downtown Chongqing and smallest in the east, shown in Fig. 5(b1).

After applying the top-down method to update SO_2 emissions, the simulation results are shown in Fig. 5(a2). Compared with the simulation results based on the baseline, the SO_2 concentration in the downtown, the west and the east respectively decreased by 78.8%, 60.0%, 35.0%. Meanwhile, the difference between the simulation results and the observations decreased more than 85% in all the counties, shown in
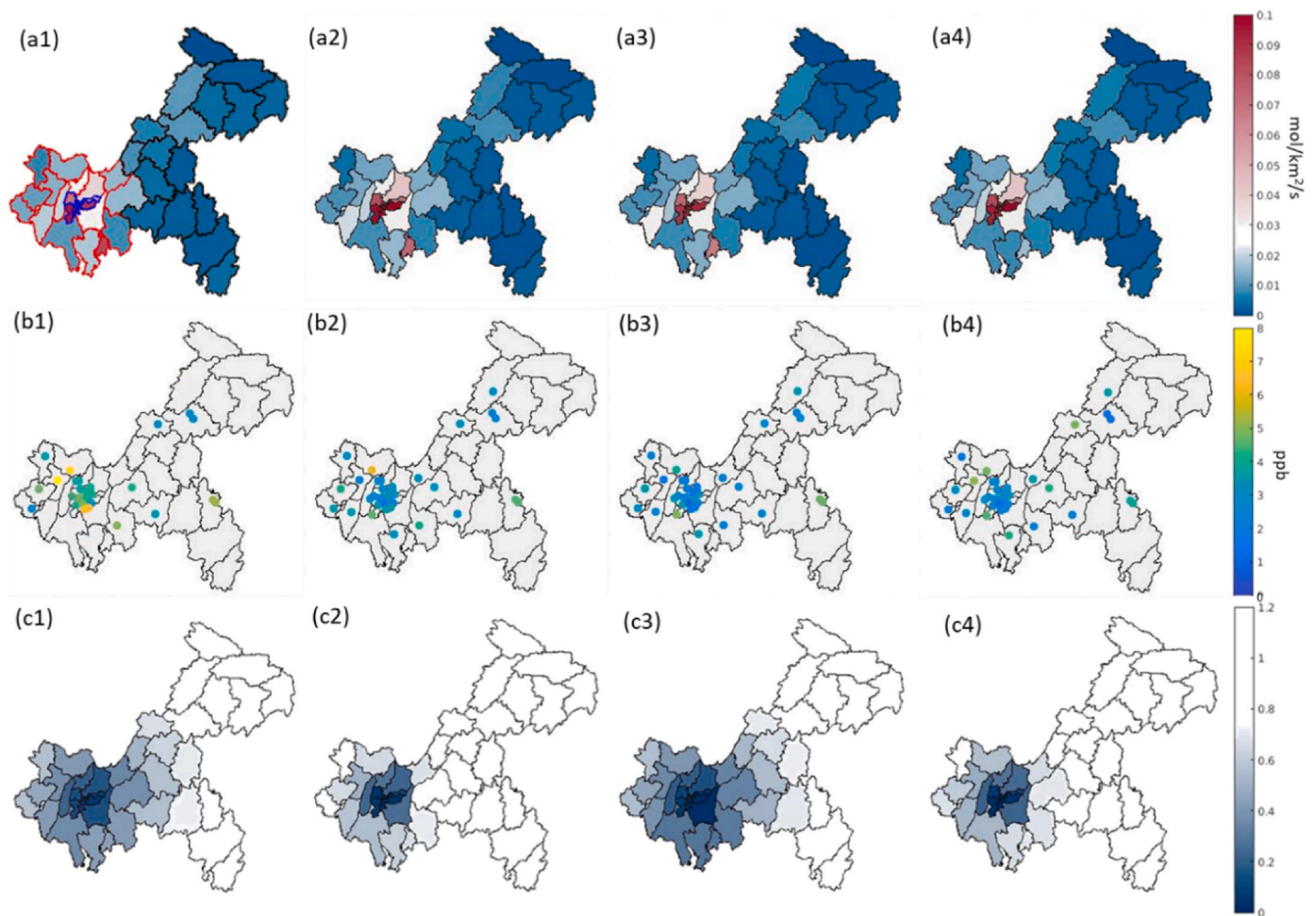
Fig. 4. Emission update with the baseline emissions and the observations. (a1) – (a4) were the profiles of baseline emissions in January, April, July and October. (b1) – (b4) were the monthly average of the observations in monitoring stations in the 4 months. (c1) – (c4) were the adjustment ratios of the updated emissions in the 4 months. The blue outline encompassed the downtown area in Figure (a1), while the red and black outlines encompassed the area of the west and east Chongqing. (For interpretation of the references to colour in this figure legend, the reader is referred to the Web version of this article).

Fig. 5(b2). The updated emissions flattened the concentration peak of SO_2 in the downtown, minimized the concentration difference between the downtown and the east, and made simulation results more comparable with the observations.

Fig. 5c shows the comparison between the observations and simulation results point by point. The simulation results with the baseline overestimated the SO_2 concentration significantly with the RMSE of 11.19. The simulation results overestimated SO_2 concentration by 611.0%, 166.4%, in the downtown and the west of Chongqing, and underestimated it by 27.0% in the east. The simulation results with the updated emissions performed better. The RMSE decreased to 1.56. The concentration in the downtown decreased significantly, overestimated by 50.7%. The concentration in the west was overestimated by 7.8% and underestimated by 38.3% in the east.

The root mean square misfit was 0.93, 1.20, 0.98, 1.32 in the four months, respectively, indicating the observations was under-fit in April and October, but slightly over-fit in January and July. The uncertainties of the observations were slightly larger in January and July than those in April and October, which caused the different fitting results.

Other statistical comparisons were shown in Table 2. The mean bias, mean gross error, root mean square error, mean fractional bias and mean fractional error described the deviations of the simulation results from the observations. Compared the difference between the observations and the simulation results with the baseline emissions, the errors and biases between the observations and the simulation results with the

updated emissions were smaller. The index of agreement and Pearson correlation coefficient showed the quality of the linear correlation between simulation results and observations. Simulation results with the updated emissions had better correlation with the observations, indicated by its larger index of agreement than that based on the simulation results with the baseline emissions. The Pearson correlation coefficient of the simulation results with the baseline emissions and the observations was slightly negative. With the updated emissions, the simulation results had a positive correlation with observations. Therefore, the updated emissions performed better in simulating concentrations of SO_2 than the baseline emissions. The definition of the metrics was given in the supplementary material.

4. Discussion

The MEIC emission inventory showed the SO_2 emissions declined in Chongqing from 2008 to 2017 (Li et al., 2017). We compared the updated emission inventory with the baseline and the latest MEIC2016 and 2017, shown in Fig. 6. The RMSE was 0.0121 between the updated emissions and MEIC2016, and 0.0074 between the updated emissions and MEIC2017. Comparing the baseline and MEIC2016 and MEIC2017, the RMSE was 0.027 and 0.0315 respectively. In general, the updated emission inventory was more comparable with MEIC2016 and 2017 than the baseline. The updated emissions were lower than the emissions of MEIC2016 and 2017 in the downtown, which also included the areas
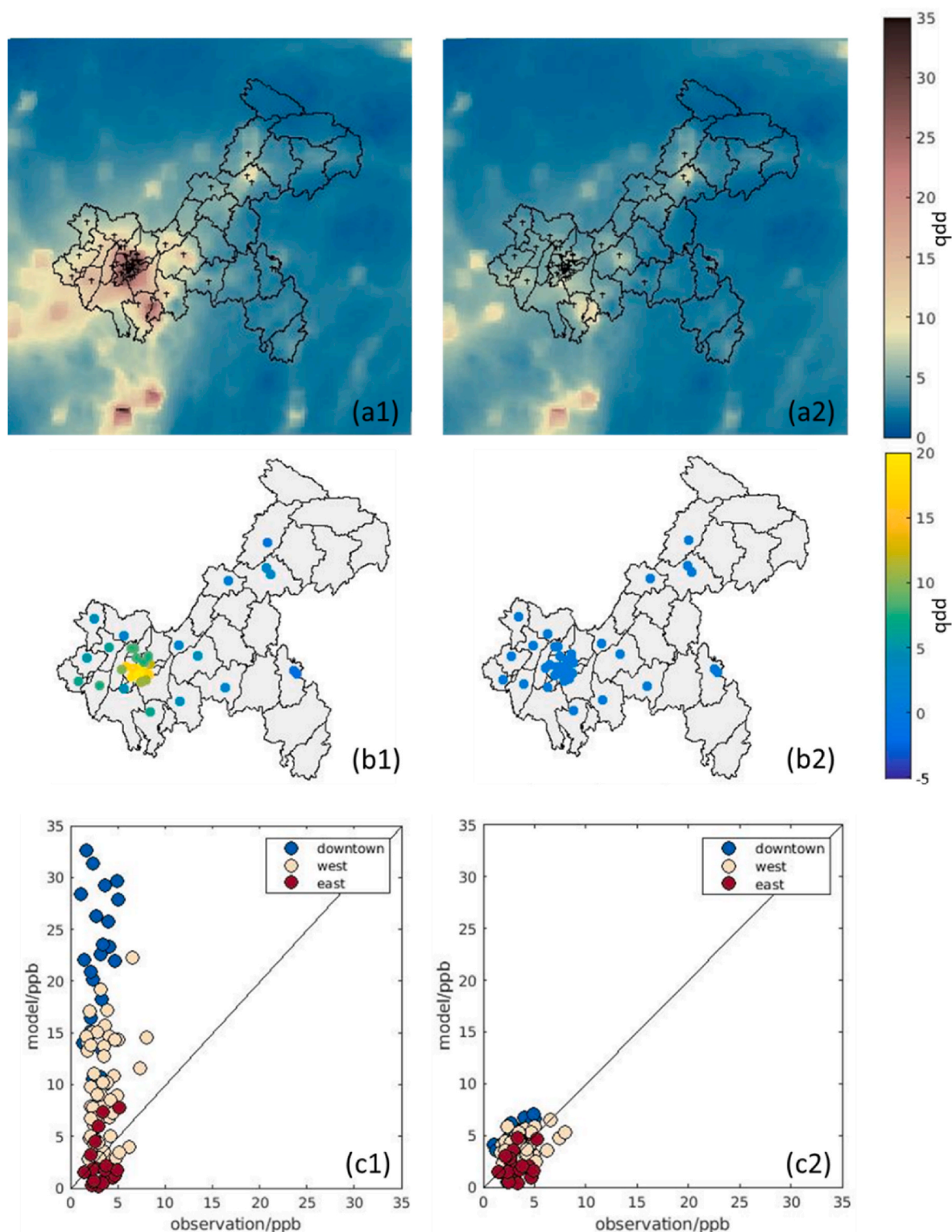
Fig. 5. Model validation. The annual average of the simulated SO$_2$ concentrations with the baseline emissions and the updated emissions was shown in (a1) and (a2). The differences between the annual average of the observations and simulation results were shown in (b1) with the baseline and (b2) with the updated emissions. Point by point comparisons of the monthly average of the observations and the simulation results were shown in (c1) with the baseline and (c2) with the updated emissions.

with the highest SO$_2$ emissions. The updated emissions were comparable with or higher than MEIC2016 and MEIC2017 in the west outside of downtown and the east in Chongqing. The emissions in the county of WanSheng were not updated much. The baseline emissions in Wan-Sheng were high, but there was no observation station in the county. We

had no constraint in updating emissions in the area. The sensitivity also showed that the influence from WanSheng on other counties were limited. Therefore, it was difficult to use the observations in other counties to update the emissions in WanSheng efficiently. In general, the updated emission inventory was in line with the declining trend of SO$_2$

Table 2

Comparison between the simulation results and observations.

	observations vs. simulation results with the baseline emissions	observations vs. simulation results with the updated emissions
mean bias (ppb)	7.76	0.43
mean gross error (ppb)	8.25	1.27
root mean square error (ppb)	11.19	1.56
mean fractional bias	0.78	0.12
mean fractional error	0.94	0.37
index of agreement	0.12	0.56
Pearson correlation coefficient	−0.002	0.30

emissions in Chongqing.

More statistical analysis on the updated emissions was shown in Table 3. The negative mean bias showed that the updated emissions were lower than the baseline emissions. The mean gross error and root mean square error both indicated that the difference between the baseline emissions and the updated emissions was the larger than the difference between the updated emissions and MEIC2016/2017, and the updated emissions were most comparable to MEIC2017. The index of agreement of the updated emissions and MEIC2017 was the largest in Table 3, which also indicated that the updated emissions had the best agreement with MEIC2017, compared with baseline emissions and MEIC2016.

The analytical solution for the Bayesian theorem was based on the assumption of linear forward Equation (7). Therefore, the linearity and deviation of the forward model should be further discussed. The simulated SO_2 concentrations from CMAQ model and the multiplication of the sensitivity matrix and the baseline emissions were compared and shown in Fig. 7. The nonlinearity was defined as the root mean square of the deviation from an ideal straight line (the diagonal) (Emancipator and Kroll, 1993). The relative nonlinearity of the 4 months was calculated as 0.058, 0.005, 0.012, 0.013, respectively. The results from January had the largest nonlinearity, followed by October. The nonlinearity in April was the smallest. The results in Fig. 7 showed that the response of SO_2 concentration to emissions was approximately linear based on CMAQ. Therefore, the assumption of the linearity was reasonable when we applied Equation (8) to update emissions of SO_2.

The mismatch between the simulation results and the observations was partially caused by the lack of constraints and influence of the baseline emissions, and affected by the errors of the model and observations. For instance, the updated emissions in WanSheng was

insufficient to capture the real emissions, which was dominated by the baseline. However, the baseline information was indispensable in the study. The sensitivity matrix shown in Fig. 3 presented the source-receptor relation. The non-zero values in the matrix accounted for a small fraction of the total entries. Therefore, the matrix was unfilled and did not provide enough details of the spatial distribution of the emissions. Considering the eigenvalue of $\mathbf{G}^T\mathbf{G}$, we found that less than 30% of the eigenvalues of $\mathbf{G}^T\mathbf{G}$ were larger than 0.1 and none of them were larger than 1. Therefore, if the baseline information was not inserted, the problem was unsolvable, because the inverse of $\mathbf{G}^T\mathbf{G}$ was required in the analytical solution.

5. Conclusion

In the present work, we updated the SO_2 emission inventory from MEIC2008 with the observations in 2021 in Chongqing.

The method to update SO_2 emissions was established. The WRF-CMAQ model provided the method to simulate SO_2 concentrations with the *a priori* knowledge of the emissions. The top-down method was adopted based on Bayesian inference, in which the sensitivity matrix was estimated by CMAQ DDM-3D model. An analytical solution of the Bayesian theorem was derived based on the linear response assumption and applied to estimate the actual SO_2 emissions.

Baseline emission inventory MEIC2008 within Chongqing was updated with the observations in 2021. The updated emissions showed a better performance in predicting SO_2 concentrations. It was time consuming to calculate the sensitivity matrix. However, the sensitivity matrix was relatively constant if the emission inventory was static in

Table 3

Comparison between the updated emissions and baseline emissions/MEIC2016/MEIC2017

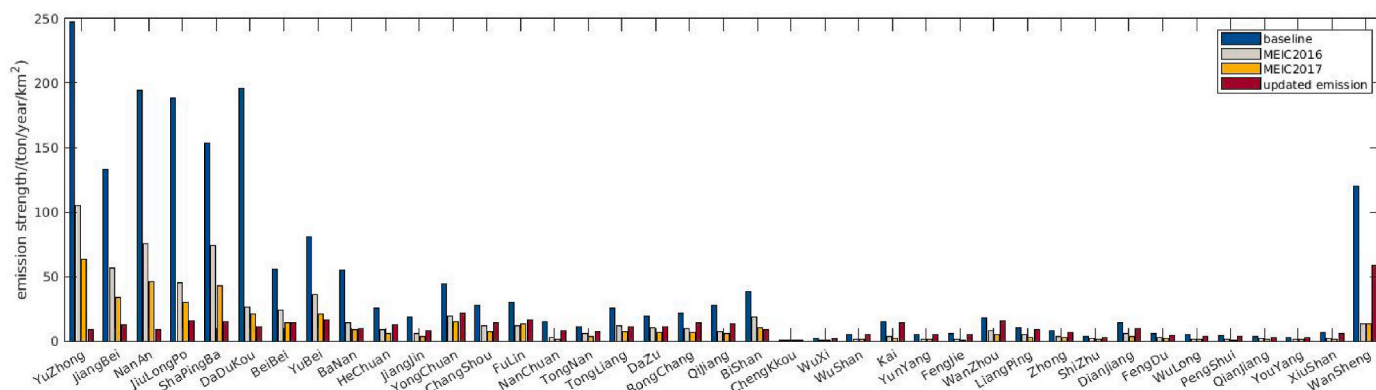|	updated emissions vs. baseline emissions	updated emissions vs. MEIC2016	updated emissions vs. MEIC2017
mean bias (mol/km^2/s)	−0.0182	−0.0028	0.0001
mean gross error (mol/km^2/s)	0.0182	0.0062	0.0045
root mean square error (mol/km^2/s)	0.0358	0.0121	0.0074
mean fractional bias	−0.66	0.23	0.58
mean fractional error	0.66	0.75	0.91
index of agreement	0.15	0.24	0.40
Pearson correlation coefficient	0.35	0.18	0.24

Fig. 6. Comparison between the updated emissions and the baseline, the latest MEIC2016 and MEIC2017 in 39 Chongqing counties.
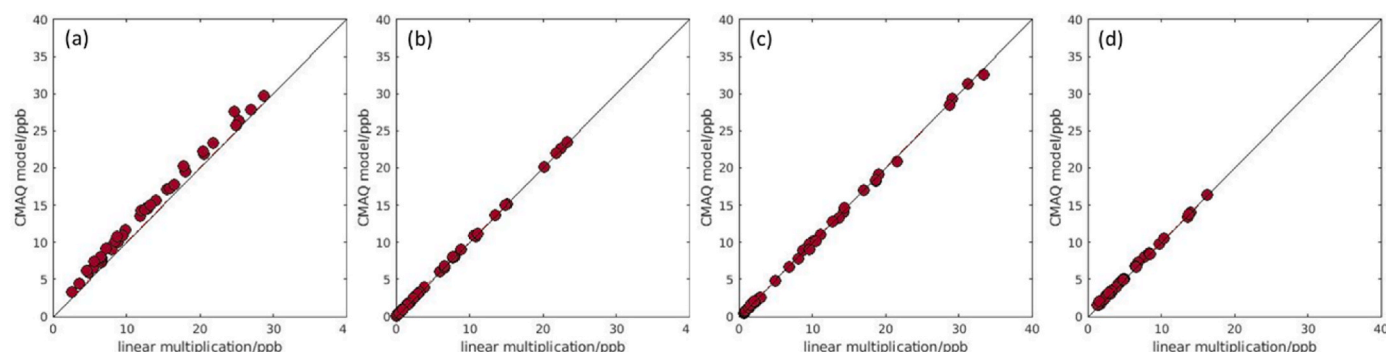
Fig. 7. Linearity of the model. The figure showed the point by point comparison between the results from the linear forward model and CMAQ model in (a) January, (b)April, (c)July, (d) October.

each month. Therefore, after obtaining the sensitivity matrix, the obsolescent emission inventory can be renewed dynamically with the real time observations.

The decline of SO_2 emissions in Chongqing can be viewed by the MEIC emission inventories over years, and also the updated emission inventory with the current observations. The nonlinearity of the forward model was discussed. The nonlinearity of the source-receptor response was quantified and showed to be small. The assumption of linearity was reasonable and practical based on CMAQ. The *a priori* knowledge of the baseline emissions was indispensable.

Overall, the adjustment of the emissions improved the accuracy in predicting SO_2 concentrations, and confirmed the declining trend on SO_2 emissions in Chongqing.

Funding

CRediT authorship contribution statement

Xiaoxiao Feng: Conceptualization, Methodology, Software, Validation, Formal analysis, Data curation, Writing – original draft. **Xiaole Zhang:** Conceptualization, Writing – review & editing. **Jing Wang:** Conceptualization, Writing – review & editing, Supervision.

Declaration of competing interest

The authors declare that they have no known competing financial interests or personal relationships that could have appeared to influence the work reported in this paper.

Data availability

Data will be made available on request.

Acknowledgments

Appendix A. Supplementary data

Supplementary data to this article can be found online at https://doi.org/10.1016/j.atmosenv.2022.119519.

References

Bae, C., Kim, H.C., Kim, B.U., Kim, Y., Woo, J.H., Kim, S., 2020. Updating Chinese SO2 emissions with surface observations for regional air-quality modeling over East Asia. Atmos. Environ. 228, 117416 https://doi.org/10.1016/j.atmosenv.2020.117416.

Bayes, T., 1763. LII. An essay towards solving a problem in the doctrine of chances. By the late Rev. Mr. Bayes, FRS communicated by Mr. Price, in a letter to John Canton, AMFR S. Phil. Trans. Roy. Soc. Lond., (53), pp.370-418. https://doi.org/10.1098/rstl.1763.0053.

Bingjiang, L., Jiming, H., Kebin, H., Fahe, C., Zhigang, X., Yuansheng, F., Zi, L., Weijun, Z., 1998. Study on designation of acid rain and SO2 pollution control areas and policy implementation. China Environ. Sci. 18 (1), 1–7.

Chang, M., 2022. SO2 pollution control: successful and transferable practices (chongqing, China). https://www.iges.or.jp/en/pub/so2-pollution-control-successful-and/en. (Accessed 30 January 2022) accessed.

Chen, B., Kan, H., 2008. Air pollution and population health: a global challenge. Environ. Health Prev. Med. 13 (2), 94–101. https://doi.org/10.1007/s12199-007-0018-5.

Cheng, X., Hao, Z., Zang, Z., Liu, Z., Xu, X., Wang, S., Liu, Y., Hu, Y., Ma, X., 2021. A new inverse modeling approach for emission sources based on the DDM-3D and 3DVAR techniques: an application to air quality forecasts in the Beijing–Tianjin–Hebei region. Atmos. Chem. Phys. 21 (18), 13747–13761. https://doi.org/10.5194/acp-21-13747-2021.

Clarke, A., Radojevic, M., 1987. Oxidation of SO2 in rainwater and its role in acid rain chemistry. Atmos. Environ. 21 (5), 1115–1123. https://doi.org/10.1016/0004-6981(87)90238-1, 1967.

Coats Jr., C.J., 1996. High-performance algorithms in the sparse matrix operator Kernel emissions (SMOKE) modeling system. In: Proc. Ninth AMS Joint Conference on Applications of Air Pollution Meteorology with A&WMA. Amer. Meteor. Soc., Atlanta, GA, pp. 584–588.

Cohan, D.S., Hakami, A., Hu, Y., Russell, A.G., 2005. Nonlinear response of ozone to emissions: source apportionment and sensitivity analysis. Environ. Sci. Technol. 39 (17), 6739–6748. https://doi.org/10.1021/es048664m.

Cohan, D.S., 2004. Applicability of CMAQ-DDM to source apportionment and control strategy development. In: 3rd Annual CMAS Models-3 Users' Conference.

Crippa, M., Guizzardi, D., Muntean, M., Schaaf, E., Dentener, F., Van Aardenne, J.A., Monni, S., Doering, U., Olivier, J.G., Pagliari, V., Janssens-Maenhout, G., 2018. Gridded emissions of air pollutants for the period 1970–2012 within EDGAR v4. 3.2. Earth Syst. Sci. Data 10 (4), 1987–2013. https://doi.org/10.5194/essd-10-1987-2018.

Dahiya, S., Anhäuser, A., Farrow, A., Thieriot, H., Kumar, A., Myllyvirta, L., 2020. Global SO2 Emission Hotspot Database, 48. Center for Research on Energy and Clean Air & Greenpeace India, Delhi.

Davis, D., 2002. A look back at the london smog of 1952 and the half century since. Environ. Health Perspect. 110 (12), A734–A735. https://doi.org/10.1289/ehp.110-a734.

Emancipator, K., Kroll, M.H., 1993. A quantitative measure of nonlinearity. Clin. Chem. 39 (5), 766–772. https://doi.org/10.1093/clinchem/39.5.766.

Feng, X., Zhang, X., He, C., Wang, J., 2021. Contributions of traffic and industrial emission reductions to the air quality improvement after the lockdown of Wuhan and neighboring cities due to COVID-19. Toxics 9, 358. https://doi.org/10.3390/toxics9120358.

Foley, K.M., Napelenok, S.L., Jang, C., Phillips, S., Hubbell, B.J., Fulcher, C.M., 2014. Two reduced form air quality modeling techniques for rapidly calculating pollutant mitigation potential across many sources, locations and precursor emission types. Atmos. Environ. 98, 283–289. https://doi.org/10.1016/j.atmosenv.2014.08.046.

Gaffney, J., Streit, G., Spall, W., Hall, J., 1987. Beyond acid rain. Do soluble oxidants and organic toxinsinteract with SO2 and NOx to increase ecosystem effects? Environ. Sci. Technol. 21 (6), 519–524. https://doi.org/10.1021/es00160a001.

Gao, M., Zhang, X., Yue, Y., Qiu, T., Wang, J., Wang, X., 2022. Air path of antimicrobial resistance related genes from layer farms: emission inventory, atmospheric transport, and human exposure. J. Hazard Mater. 430, 128417 https://doi.org/10.1016/j.jhazmat.2022.128417.

Hakami, A., Odman, M.T., Russell, A.G., 2003. High-order, direct sensitivity analysis of multidimensional air quality models. Environ. Sci. Technol. 37 (11), 2442–2452. https://doi.org/10.1021/es020677h.

Helfand, W., Lazarus, J., Theerman, P., 2001. Donora, Pennsylvania: an environmental disaster of the 20th century. Am. J. Publ. Health 91 (4). https://doi.org/10.2105/ajph.91.4.553, 553-553.

Henne, S., Brunner, D., Oney, B., Leuenberger, M., Eugster, W., Bamberger, I., Meinhardt, F., Steinbacher, M., Emmenegger, L., 2016. Validation of the Swiss methane emission inventory by atmospheric observations and inverse modelling. Atmos. Chem. Phys. 16 (6), 3683–3710. https://doi.org/10.5194/acp-16-3683-2016.

Hiller, R.V., Bretscher, D., DelSontro, T., Diem, T., Eugster, W., Henneberger, R., Hobi, S., Hodson, E., Imer, D., Kreuzer, M., Künzle, T., 2014. Anthropogenic and natural methane fluxes in Switzerland synthesized within a spatially explicit inventory. Biogeosciences 11 (7), 1941–1959. https://doi.org/10.5194/bg-11-1941-2014.

Hong, C., Zhang, Q., He, K., Guan, D., Li, M., Liu, F., Zheng, B., 2017. Variations of China's emission estimates: response to uncertainties in energy statistics. Atmos. Chem. Phys. 17 (2), 1227–1239. https://doi.org/10.5194/acp-17-1227-2017.

Itahashi, S., Uno, I., Kim, S., 2012. Source contributions of sulfate aerosol over East Asia estimated by CMAQ-DDM. Environ. Sci. Technol. 46 (12), 6733–6741. https://doi.org/10.1021/es300887w.

Jain, R., 2015. Environmental Impact of Mining and Mineral Processing: Management, Monitoring, and Auditing Strategies. Butterworth-Heinemann.

Kurokawa, J., Ohara, T., 2020. Long-term historical trends in air pollutant emissions in Asia: regional Emission inventory in ASia (REAS) version 3. Atmos. Chem. Phys. 20, 12761–12793. https://doi.org/10.5194/acp-20-12761-2020.

Larssen, T., Lydersen, E., Tang, D., He, Y., Gao, J., Liu, H., Duan, L., Seip, H.M., Vogt, R. D., Mulder, J., Shao, M., 2006. Acid rain in China. Environ. Sci. Technol. 40 (2), 418–425. https://doi.org/10.1021/es0626133.

Lee, C., Martin, R.V., van Donkelaar, A., Lee, H., Dickerson, R.R., Hains, J.C., Krotkov, N., Richter, A., Vinnikov, K., Schwab, J.J., 2011. SO2 emissions and lifetimes: estimates from inverse modeling using in situ and global, space-based (SCIAMACHY and OMI) observations. J. Geophys. Res. Atmos. 116 (D6) https://doi.org/10.1029/2010JD014758.

Li, M., Liu, H., Geng, G., Hong, C., Liu, F., Song, Y., Tong, D., Zheng, B., Cui, H., Man, H., Zhang, Q., He, K., 2017. Anthropogenic emission inventories in China: a review. Natl. Sci. Rev. 4, 834–866. https://doi.org/10.1093/nsr/nwx150.

Mazzanti, M., Musolesi, A., Zoboli, R., 2006. A bayesian approach to the estimation of environmental kuznets curves for CO2 emissions. FEEM Working. https://doi.org/10.2139/ssrn.936903. Paper No. 121.06.

Olivier, J.G.J., Bouwman, A.F., van der Maas, C.W.M., 1994. Emission database for global atmospheric research (Edgar). Environ. Monit. Assess. 31, 93–106. https://doi.org/10.1007/BF00547184.

ORNL DAAC, 2018. MODIS and VIIRS land products global subsetting and visualization tool. ORNL DAAC, oak ridge, Tennessee, USA. Subset obtained for MOD13Q1 product at various sites in Spatial Range: N=53.33N, S=3.51N, E=135.05E, W=73.33E, time period: 2021-01-01 to 2021-10-31, and subset size: 5 x 5 km. https://doi.org/10.3334/ORNLDAAC/1379. Accessed January 30, 2022.

Pandey, J., Kumar, R., Devotta, S., 2005. Health risks of NO2, SPM and SO2 in Delhi (India). Atmos. Environ. 39 (36), 6868–6874. https://doi.org/10.1016/j.atmosenv.2005.08.004.

Popp, D., 2006. International innovation and diffusion of air pollution control technologies: the effects of NOX and SO2 regulation in the US, Japan, and Germany. J. Environ. Econ. Manag. 51 (1), 46–71. https://doi.org/10.1016/j.jeem.2005.04.006.

Qu, Z., Henze, D.K., Li, C., Theys, N., Wang, Y., Wang, J., Wang, W., Han, J., Shim, C., Dickerson, R.R., Ren, X., 2019. SO2 emission estimates using OMI SO2 retrievals for 2005–2017. J. Geophys. Res. Atmos. 124 (14), 8336–8359. https://doi.org/10.1029/2019JD030243.

Shen, H., Huang, Y., Wang, R., Zhu, D., Li, W., Shen, G., Wang, B., Zhang, Y., Chen, Y., Lu, Y., Chen, H., Li, T., Sun, K., Li, B., Liu, W., Liu, J., Tao, S., 2013. Global atmospheric emissions of polycyclic aromatic hydrocarbons from 1960 to 2008 and future predictions. Environ. Sci. Technol. 47 (12), 6415–6424. https://doi.org/10.1021/es400857z.

Skamarock, W.C., Klemp, J.B., Dudhia, J., Gill, D.O., Barker, D.M., Duda, M.G., Huang, X.-Y., Wang, W., Powers, J.G., 2008. A description of the advanced research WRF version 3. NCAR Tech. Note NCAR/TN-475+STR 113. https://doi.org/10.5065/D68S4MVH.

Streets, D., Waldhoff, S., 2000. Present and future emissions of air pollutants in China. Atmos. Environ. 34 (3), 363–374. https://doi.org/10.1016/s1352-2310(99)00167-3.

Tarantola, A., Valette, B., 1982. Generalized nonlinear inverse problems solved using the least squares criterion. Rev. Geophys. 20 (2), 219–232. https://doi.org/10.1029/RG020i002p00219.

Thompson, R.L., Stohl, A., Zhou, L.X., Dlugokencky, E., Fukuyama, Y., Tohjima, Y., Kim, S.Y., Lee, H., Nisbet, E.G., Fisher, R.E., Lowry, D., 2015. Methane emissions in East Asia for 2000–2011 estimated using an atmospheric Bayesian inversion. J. Geophys. Res. Atmos. 120 (9), 4352–4369. https://doi.org/10.1002/2014JD022394.

United States Environmental Protection Agency, 2020. CMAQ. https://doi.org/10.5281/zenodo.1167892 [Software], Version 5.3.2.

Venners, S., Wang, B., Xu, Z., Schlatter, Y., Wang, L., Xu, X., 2003. Particulate matter, sulfur dioxide, and daily mortality in Chongqing, China. Environ. Health Perspect. 111 (4), 562–567. https://doi.org/10.1289/ehp.5664.

Wang, Y., Huang, H., Huang, L., Zhang, X., 2018. Source term estimation of hazardous material releases using hybrid genetic algorithm with composite cost functions. Eng. Appl. Artif. Intell. 75, 102–113. https://doi.org/10.1016/j.engappai.2018.08.005.

Whelpdale, D.M., Kaiser, M.S., 1997. Global Acid Deposition Assessment. World Mereorological Organization (WMO).

Xuan, C., Xiaoran, S., Zhaoji, S., Jiaen, Z., Zhong, Q., Huimin, X., Hui, W., 2021. Analysis of the spatio-temporal changes in acid rain and their causes in China (1998–2018). Journal of Resources and Ecology 12 (5). https://doi.org/10.5814/j.issn.1674-764x.2021.05.002.

Zhang, J., Zhang, S., Zhang, X., Wang, J., Wu, Y., Hao, J., 2022. Developing a high-resolution emission inventory of China's aviation sector using real-world flight trajectory data. Environ. Sci. Technol. 56, 5743–5752. https://doi.org/10.1021/acs.est.1c08741.

Zhang, X.L., Su, G.F., Yuan, H.Y., Chen, J.G., Huang, Q.Y., 2014. Modified ensemble Kalman filter for nuclear accident atmospheric dispersion: Prediction improved and source estimated. J. Hazard Mater. 280, 143–155. https://doi.org/10.1016/j.jhazmat.2014.07.064.

Zhang, X.L., Su, G.F., Chen, J.G., Raskob, W., Yuan, H.Y., Huang, Q.Y., 2015. Iterative ensemble Kalman filter for atmospheric dispersion in nuclear accidents: an application to Kincaid tracer experiment. J. Hazard Mater. 297, 329–339. https://doi.org/10.1016/j.jhazmat.2015.05.035.

Zhang, X.L., Chen, X., Wang, J., 2019. A number-based inventory of size-resolved black carbon particle emissions by global civil aviation. Nat. Commun. 10, 534. https://doi.org/10.1038/s41467-019-08491-9.

Zhang, X., Karl, M., Zhang, L., Wang, J., 2020. Influence of aviation emission on the particle number concentration near Zurich airport. Environ. Sci. Technol. 54, 14161–14171. https://doi.org/10.1021/acs.est.0c02249.

Zhang, X., Ji, Z., Yue, Y., Liu, H., Wang, J., 2021. Infection risk assessment of COVID-19 through aerosol transmission: a case study of South China seafood market. Environ. Sci. Technol. 55, 4123–4133. https://doi.org/10.1021/acs.est.0c02895.

Zheng, B., Zhang, Q., Tong, D., Chen, C., Hong, C., Li, M., Geng, G., Lei, Y., Huo, H., He, K., 2017. Resolution dependence of uncertainties in gridded emission inventories: a case study in Hebei, China. Atmos. Chem. Phys. 17 (2), 921–933. https://doi.org/10.5194/acp-17-921-2017.